Elaboration of capsules from Pickering double emulsion polymerization stabilized solely by cellulose nanocrystals

Hanaé Dupont, Valérie Héroguez, Véronique Schmitt

▶ **To cite this version:**

Hanaé Dupont, Valérie Héroguez, Véronique Schmitt. Elaboration of capsules from Pickering double emulsion polymerization stabilized solely by cellulose nanocrystals. Carbohydrate Polymers, 2021, 279, pp.118997. 10.1016/j.carbpol.2021.118997 . hal-03771246

HAL Id: hal-03771246
https://hal.science/hal-03771246

Submitted on 8 Sep 2022

HAL is a multi-disciplinary open access archive for the deposit and dissemination of scientific research documents, whether they are published or not. The documents may come from teaching and research institutions in France or abroad, or from public or private research centers.

L'archive ouverte pluridisciplinaire **HAL**, est destinée au dépôt et à la diffusion de documents scientifiques de niveau recherche, publiés ou non, émanant des établissements d'enseignement et de recherche français ou étrangers, des laboratoires publics ou privés.

Elaboration of capsules from Pickering double emulsion polymerization stabilized solely by cellulose nanocrystals

Hanaé Dupont[1,2], Valérie Héroguez[2,*], Véronique Schmitt[1,*]

[1] Centre de Recherche Paul Pascal, UMR 5031 Univ. Bordeaux, CNRS, 115 avenue du Dr Albert Schweitzer, 33600 Pessac, France.

[2] Laboratoire de Chimie des Polymères Organiques, Univ. Bordeaux, CNRS, Bordeaux INP, UMR 5629, Bordeaux, 16 Avenue Pey-Berland, F-33607 Pessac, France.

* corresponding authors

veronique.schmitt@crpp.cnrs.fr

heroguez@enscbp.fr

Abstract

Pickering double oil-in-water-in-oil emulsions O/W/O were stabilized using solely cellulose nanocrystals (CNCs), which were modified by introducing surface brominated functions. The emulsions were formulated using only bio-friendly components, among which isopropyl myristate as oil phase, hydroxyl oligoethylene glycol methacrylate (OEGMA) as macromonomer, tetraethylene glycol diacrylate (TEGDA) as cross-linker, and CNCs as stabilizing particles. Formulation parameters could be tuned easily to modulate the fraction of inner emulsion droplets within the double emulsion drops or change the monomer(s) composition within the aqueous phase. The latter was further polymerized to synthesize matrix capsules. The obtained objects showed good resistance to the vacuum and were efficiently used as promising encapsulation vessels. Both hydrophobic and hydrophilic model dyes were encapsulated, with an encapsulation efficiency of about 90%.

Keywords: Pickering, cellulose, oil-in-water-in-oil, polymerization, encapsulation

1. Introduction

Emulsions are metastable systems and are defined as the mixture of at least two immiscible liquids. Therefore, their kinetic stabilization requires the use of stabilizing agents, like surfactants, polymers or particles. A rising interest has been put towards the use of particles and the study of the related Pickering emulsions to replace the widely used (macro)molecular scale surfactants (Arditty et al., 2004; Gonzalez Ortiz et al., 2020). Pickering emulsions were discovered by Pickering (Pickering, 1907) and Ramsden (Ramsden, 1904) in the early 1900's and have regained interest since the 2000's because of their high kinetic stability and ease of implementation. According to rising environmental and transparency concerns, the use of organic particles with natural origin as renewable and harmless stabilizers has been considered (Dupont, Maingret, et al., 2021; Sarkar & Dickinson, 2020). Among them, cellulose nanocrystals (CNCs) appear as particles with high potential because they are biosourced and highly available, they are biodegradable and they exhibit a well-known functionalized structure that offers an easily modifiable surface. Studies have shown that they efficiently stabilize direct oil-in-water (O/W) (Deng et al., 2018; Gestranius et al., 2017; Hedjazi & Razavi, 2018; Kalashnikova et al., 2011; Mackie et al., 2019) and inverse water-in-oil (W/O) (Dupont, Laurichesse et al, 2021 ; Guo et al., 2017; Lee et al., 2013; Zhang et al., 2018) Pickering emulsions. However, the occurrences in the literature of more complex systems such as multiple emulsions are still scarce. In most cases, only one of the two interfaces is stabilized by natural organic particles, the other being stabilized by surfactants. This was indeed the case in the study of Matos *et al.* (Matos et al., 2013) who used starch nanoparticles to stabilize the outer interface of water-in-oil-in-water (W/O/W) emulsions, along with a hydrophobic polyglycerol polyricinoleate (PGPR) for the inner interface. More recently, scarce studies reporting double emulsions stabilized solely by particles with natural origin were published. Spyropoulos *et al.* (Spyropoulos et al., 2019) showed good stability of W/O/W emulsions stabilized by rutin particles for the O/W interface, and nanocellulose for the W/O interface, and Cunha *et al.* (Cunha et al., 2014) formulated an O/W/O (oil-in-water-in-oil) emulsions fully stabilized by cellulose derivatives (CNC and/or CNF). Both works focused on the formulation

of the double emulsion system as a proof of concept, but did not used it for any particular application. The only example of application of such systems was demonstrated by Pan *et al.*, who used lignin particles to produce a W/O/W double emulsions, which intermediate phase was further polymerized to produced porous absorbent beads (Pan et al., 2015). Hence, we here propose to investigate further the potential of Pickering double emulsions stabilized solely with cellulose nanocrystals as polymeric vessels for encapsulation. CNCs of both interfaces were submitted to the same modification process, their modification rate being the only variable to modulate their wettability. In the present work, O/W Pickering emulsion was stabilized using hydrophilic CNCs. This direct emulsion was then used as dispersed phase for a second emulsification step to produce an O/W/O Pickering double emulsion stabilized by hydrophobic CNCs, using isopropyl myristate as a biocompatible oil phase. Based on a preliminary study conducted on W/O emulsions (Dupont, Laurichesse, et al., 2021), the intermediate aqueous phase of the double emulsion, composed of hydroxyl oligoethylene glycol methacrylate (OEGMA) and an potential cross-linker (tetraethylene glycol diacrylate, TEGDA), was subsequently polymerized by free radical polymerization to obtain solid capsules as schematically depicted in Figure 1. The resulting objects were further proven efficient encapsulation vessels for both hydrophobic and hydrophilic model dyes, showing the high applicative potential of these objects.

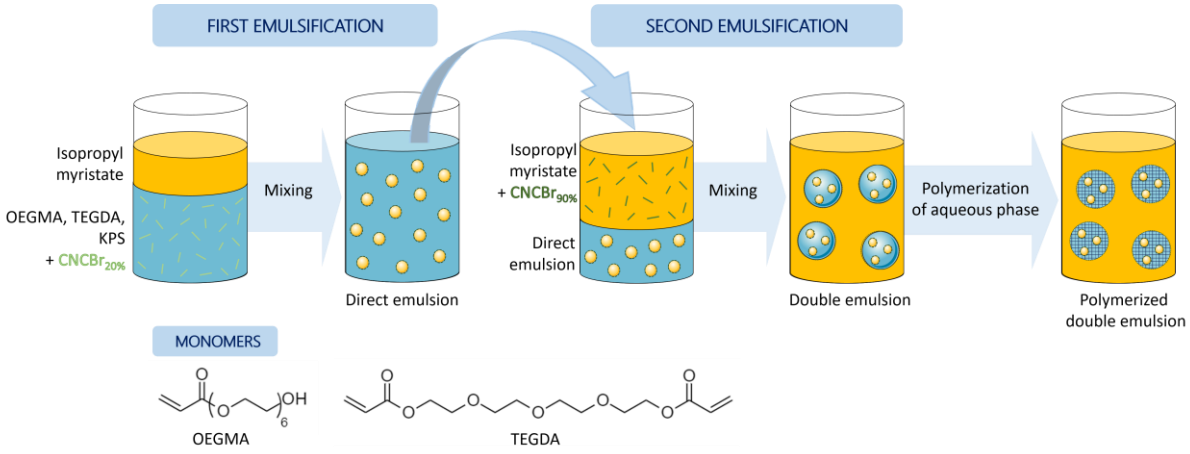

Figure 1: Principle scheme for the two-step emulsification and synthesis of the polymerized double O/W/O emulsions.

2. Experimental

2.1 Materials

Pristine CNCs were purchased from The University of Maine, under freeze-dried CNC form, isolated from sulfuric acid hydrolysis of wood pulp. The crystals present initially on their surface both sulfate (1.05 wt% as data from the provider) and hydroxyl functions (3.10 ± 0.11 mmol.g^{-1} of CNC). The initial CNCs exhibited a rod-like shape with estimated dimension of L=138 ± 47 nm in length and l=25 ± 6 nm in width based on AFM analysis (Dupont et al., 2020; Dupont, Laurichesse, et al., 2021).

Triethylamine (TEA) (Fisher scientific, 99%), α-bromoisobutyryl bromide (Bibb) (ABCR, 98%), dimethylaminopyridine (DMAP) (Sigma Aldrich, 99%) were used for the CNC modification without any purification. Isopropyl myristate (IPM) (98%, Alfa Aesar), an oil allowed for cosmetic applications, was used as received as the oil phase for all the emulsion systems. Hydroxyl oligoethylene glycol methacrylate (OEGMA, M_n = 360 g/mol) (Sigma Aldrich), tetraethylene glycol diacrylate (TEGDA) (Sigma Aldrich) were used as macromonomer and cross-linker without purification. Potassium persulfate (KPS) (>99%, Sigma Aldrich) was used as received. Fluorescent yellow (FY131SC) (Dow Chemicals) containing Solvent Red 175, methylene blue (Fluka) and toluidine blue (Acros) were used as fluorescent dyes.

2.2 CNC-Br synthesis

CNC-Br synthesis was first described by Meng *et al.* (Meng et al., 2008) and Morandi *et al.* (Morandi et al., 2009), modified by Werner *et al.* (Werner et al., 2019) and optimized in the present work. 2 g of CNC and 2 g of DMAP were introduced in a double-wall reactor. After a nitrogen purge, 100 mL of dry DMF were added to the powders under gentle agitation with a magnetic stirrer. The solution was cooled down to 0°C. 8.5 g (1.48 mol/L) of Bibb (reactant) and 4.8 g (1.90 mol/L) of TEA, were added to the solution under vigorous agitation. After 3 h for the least modified and 41 h for the most modified, CNC-Br were precipitated in 200 mL of a mixture of THF/ethanol (50/50$_{v/v}$), isolated by centrifugation (6000 rpm, 10 min, 15°C) and redispersed in water. For a short modification time, that means a low modification rate (3 h, particles noted CNC-Br$_{20\%}$), the aqueous suspension of CNC-Br was dialyzed against pure

105 water during 7 days with a 1 kDa membrane. For a long modification time, that means a high
106 modification rate (41 h, particles noted CNC-$Br_{90\%}$), the purification procedure was different.
107 THF was subsequently added to the CNC-Br aqueous dispersion before centrifugation, in a
108 ratio 1:1. This step was repeated at least 3 times to remove all unreacted species. For both
109 modification times, the final dispersion in water was freeze-dried to obtain a powder.
110 The grafting was confirmed by CP MAS NMR and FT-IR by following the appearance of the
111 stretching bonds corresponding to the surface ester groups at 1760 cm^{-1} (v(C=O)) and 1060
112 cm^{-1} (v(C-O)) (Fig. S1, SI). Quantitative evaluation of modification rates was determined by
113 elemental analysis thanks to the mass percentage of bromine and the amount of surface
114 hydroxyl groups (Eq. 1).

115 $$\%\ substitution = \frac{mmol\ of\ Br\ by\ gram\ of\ CNCs}{mmol\ of\ surface\ hydroxyl\ functions\ by\ gram\ of\ CNCs} = \frac{n_{Br}}{n_{OH}}.100 \qquad \textit{Eq. 1}$$

116 with n_{OH} = 3.10 mmol/g, estimated in a previous study (Brand et al., 2017).

117 **2.3 Emulsion formulation and characterization**

118 **2.3.1 Direct emulsion**

119 The 3 mL aqueous continuous phase was composed of a polymerization system and CNC-
120 $Br_{20\%}$ (ranging from 5 to 25 g/L of dispersed phase). The polymerization system was composed
121 of OEGMA (concentration ranging from 10 wt% to 40 wt% with respect to the aqueous phase),
122 possibly a cross-linker TEGDA (15 mol% compared to the total amount of macromonomer,
123 equivalently 5 wt% compared to the aqueous solution) diluted in salted water (NaCl, 40
124 mmol/L) and the free radical initiator KPS (1 g/100 g (macro)monomer(s)). CNC-$Br_{20\%}$ were
125 dispersed in the polymerization medium using an ultrasonic bath for 2 min and a Bioblock
126 vibra-cell equipped with an ultrasonic tip during 15 s (cycles of 3 s “on” at 20 % power and 3 s
127 “off”). 1 mL of IPM was added to the aqueous suspension and mixed using the ultrasonic tip
128 during 15 s (cycles of 3 s “on” at 30 % power and 3 s “off”) to obtain an oil-in-water direct
129 emulsion.

Emulsion droplet size distribution was obtained by measuring the diameter of a hundred droplets using ImageJ software processing on optical microscopy images. The droplet surface-average diameter, or Sauter diameter $D_{3,2}$ was calculated as follow (Eq. 2):

$$D_{3,2} = \frac{\sum_i N_i D_i^3}{\sum_i N_i D_i^2} \quad \textit{Eq. 2}$$

Where N_i is the number of droplets with diameter D_i. The standard deviation was also calculated as follow (Eq. 3):

$$S = \sqrt{\frac{\sum_1^n (D_i - D_{3,2})^2}{n}} \quad \textit{Eq. 3}$$

2.3.2 Double emulsion

The continuous phase was prepared by mixing 3 mL of IPM with CNC-$Br_{90\%}$ (ranging from 5 to 20 g/L with respect to the amount of direct emulsion) with an ultrasonic bath for 2 min. 1 mL of the previously described direct emulsion was incorporated to the oil-CNC mixture using a vortex at 1500 rpm for 30 s. The double emulsion drop size was assessed identically as for the direct emulsion using Eq. 2 and Eq. 3. In the following, droplet denomination will refer to the inner emulsion, whereas the term drop will refer to the external one.

2.4 Double emulsion polymerization and characterization

The double emulsions were placed in an oil bath at 75°C for 24h. The emulsion drop size distribution after polymerization was controlled by optical microscopy using Eq. 2 and Eq. 3. A sample of the polymerized double emulsions was then washed with EtOH and dried to assess the morphology by scanning electron microscopy (SEM). In the following, the polymerized double emulsions will be referred as capsules.

2.5 Dye encapsulation within the double emulsion

The hydrophobic dye FY131SC was diluted in IPM to reach a concentration of 0.002 wt%. The hydrophilic dye, toluidine blue, was diluted in salted water (NaCl, 40 mmol/L) to reach a concentration of 0.02 wt%. This solution was used for the (macro)monomer(s) dilution to formulate the stained aqueous phase of the emulsion. The direct emulsion was formulated with the two previously described oil and aqueous phases. This emulsion was then incorporated

into regular IPM to obtain the double emulsion. Both direct and double emulsions were observed using a confocal microscope equipped to assess the effective encapsulation of both dyes.

The encapsulation efficiency (EE) was measured from double emulsions containing only FY131SC in the inner IPM droplets. 500 µL of the continuous supernatant IPM was taken from the double emulsion and diluted in 500 µL of regular IPM. The mixture was then filtered and analyzed by UV-visible spectrophotometry. The EE was calculated as (Eq. 4):

$$\text{Encapsulation efficiency}\ (\%) = \left(1 - \frac{amount\ of\ dye\ in\ the\ continuous\ phase}{total\ amount\ of\ dye\ in\ the\ double\ emulsion}\right) * 100 \quad \textit{Eq. 4}$$

2.6 Instrumentation

Infrared spectra of unmodified and brominated CNCs were recorded using a Vertex 70 Bruker FT-IR spectrometer. CNC powder was analyzed thanks to an attenuated total reflectance ATR accessory. Each spectrum was recorded between 4000 cm^{-1} and 400 cm^{-1} with a resolution of 4 cm^{-1} with 32 scans.

Optical micrographs were taken on a bright-field upright microscope (Zeiss Axioscope 40) with an Axioscope 105 color camera. Emulsions were placed onto a glass slide, then a spacer was used to avoid compression of the droplets during observation, finally the sample was covered by a lamella. The recorded images were analyzed with ImageJ.

Scanning electron microscopy (SEM) observations were performed with a HITACHI TM-1000 apparatus operating at 15 kV. Samples were coated with a layer of Au-Pd before observation using a plasma at 10 mA for 30 s.

All confocal microscopy images were acquired on a Leica TCS SP5 (Leica Microsystems CMS GmbH, Mannheim, Germany) inverted confocal microscope (DMI6000).

UV-visible spectrophotometry was performed using a Cary 100 UV-vis spectrophotometer between 400 nm and 800 nm, in 500 µL quartz cells.

Contact angles were measured on a Teclis apparatus using the drop deposit technique. Pellets of CNCs were produced from 200 mg of dry material using a 13 mm Evacuable Pellet Die and a manual hydraulic press (5 tons during 1 min). The pellets were kept dry in an oven at 50 °C

prior to experiment. Drops of salted water (4 µL) were deposited on the pellets and the contact angle was measured. For each CNC modification rate, the contact angle was measured at least three times.

3. Result and discussion

3.1 CNC modification

The CNC were modified using Bibb, enabling the grafting of brominated moieties often used for the initiation of controlled radical polymerization like ATRP, as demonstrated in a previous study (Dupont, Laurichesse, et al., 2021). Here, the grafting was only used in order to increase the overall hydrophobicity of the CNCs. The CNC modification rate of hydroxyl functions into brominated hydrophobic moieties could be controlled by adjusting the reaction time. The more time the reactants were in contact with the CNCs the more hydroxyl functions were esterified, leading to more hydrophobic CNCs. As a consequence, the modification rate functions could be plotted against the reaction time, showing a linear increase in brominated functions followed by a plateau when reaching 100% of hydroxyl substituted by brominated function for at least 40 h of reaction (Figure 2A).

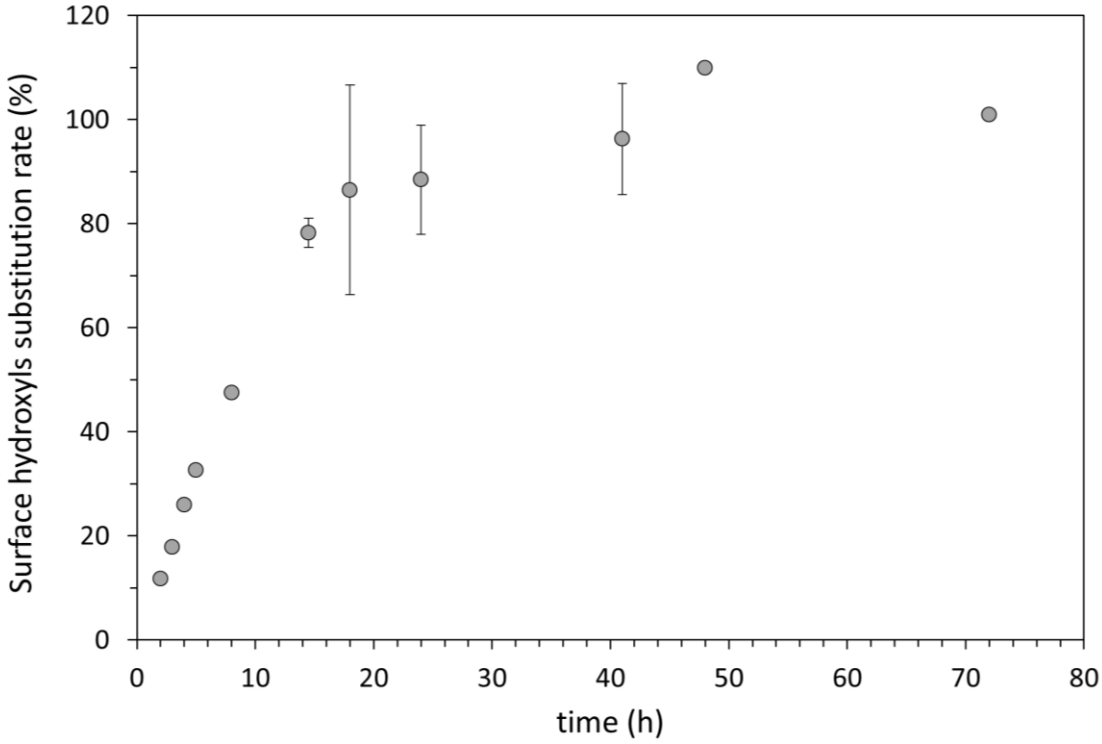

B)

Modification features	$CNC\text{-}Br_{20\%}$	$CNC\text{-}Br_{90\%}$
Duration of the reaction (h)	3	41
%wt of Br	4.43	21.98
mmol of Br per gram of CNC	0.55	2.75
OH substitution rate at the CNC surface (%)	18	89

C)

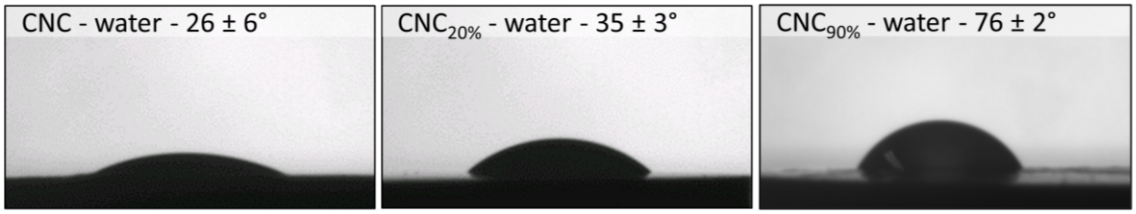

Figure 2: A) CNC surface modification rate as a function of the reaction time. Error bars represent the repeatability of the experiment for a given reaction time. B) Characteristics of the two modified CNC batches used in this study. C) Contact angle between water, CNC surfaces and air.

It has been observed that for low modification rates (up to 50%), the CNCs were still hydrophilic enough to be dispersed in water and to stabilize efficiently direct O/W emulsions. Moreover, the surface modification performed on the CNCs enhanced their ability to adsorb at oil-water interfaces, making them more suitable Pickering emulsion stabilizers, compared to pristine crystals. On the contrary, above 50% of modification the CNCs become more hydrophobic and

can only be dispersed into hydrophobic solvents or oils (Destribats et al., 2014; Finkle et al., 1923). Following Finkle's law, they indeed efficiently stabilize inverse W/O emulsions.

In the present study, we chose to work with two sets of surface-modified CNCs, suitable for the stabilization of direct and inverse emulsions. Two batches of CNCs were therefore modified during 3 h and 41 h respectively to reach modification rates of approximately 20% and 90% (Figure 2A, Figure 2B). They are noted CNC-$Br_{20\%}$ and CNC-$Br_{90\%}$ respectively.

To further characterize the chemical modification and hydrophilic-lipophilic balance of the CNCs, water contact angles were measured for pristine CNCs and the two CNC-Br batches (Figure 2C). Water droplets were deposited onto the CNC pellets, showing an increase in the contact angle with the increase of brominated moieties. Pristine CNCs exhibited a low contact angle of 26 ± 6° consistent with their intrinsic hydrophilic nature. For low modification rate, the contact angle value increased to 35 ± 3°, showing that the CNC-$Br_{20\%}$ are more hydrophobic than their pristine form, but are still quite hydrophilic, as they can be redispersed in water. On the contrary, for high modification rates as for CNC-$Br_{90\%}$, the contact angle increased by 50° compared to pristine particles, up to 76 ± 2°, showing the great impact of the surface modification on the hydrophilic/hydrophobic behavior. It is worth noting that this three-phase-contact-angle was measured between CNCs, water and air, which allows a comparison between the different CNCs but does not give the three phase contact angle of the system used in the emulsions: it is therefore useful as a comparative method but does not represent the present system, as the monomer and the oil are missing from this measurement.

3.2 Emulsion formulation

3.2.1 Direct emulsion O/W

Emulsions components were chosen in order to formulate an overall bio-friendly system. IPM was used as oil phase, as a non-toxic biocompatible oil already used in cosmetic and pharmaceutic applications. Regarding the aqueous phase, the polymerization system was selected similarly using biocompatible functionalized polyethylene glycol derivatives, OEGMA and TEGDA. The metastable emulsion was then stabilized using biosourced CNCs.

Emulsion formulation parameters were determined based on previous optimization on simple inverse emulsions (Dupont, Laurichesse, et al., 2021). Hence, the concentration of OEGMA was set to 10, 35 or 40 wt% of the aqueous phase, and the possible addition of TEGDA as a cross-linker was set to 15 mol% with regard to the total (macro)monomers concentration (which is equivalent to a composition of 35 wt% of OEGMA and 5 wt% of TEGDA with respect to the aqueous solution). Oil-to-water volume fraction could be tuned, and O/W emulsions were formulated with fraction of 25/75 or 50/50, which will enable later the variation of inner droplets concentration for the double emulsion loading.

Stable direct O/W Pickering emulsions were obtained using CNC-$Br_{20\%}$ particles as stabilizers, as they were mainly hydrophilic and could lead to the stabilization of direct emulsion following Finkle's rule (Finkle et al., 1923). The concentration in OEGMA was set to 40 wt%, and the concentration in stabilizing particles was varied from 5 to 25 g/L with respect to the oil phase. The Sauter diameter was measured for each sample and its inverse ($1/D_{3,2}$) was plotted against the CNC-$Br_{20\%}$ concentration (Figure 3).

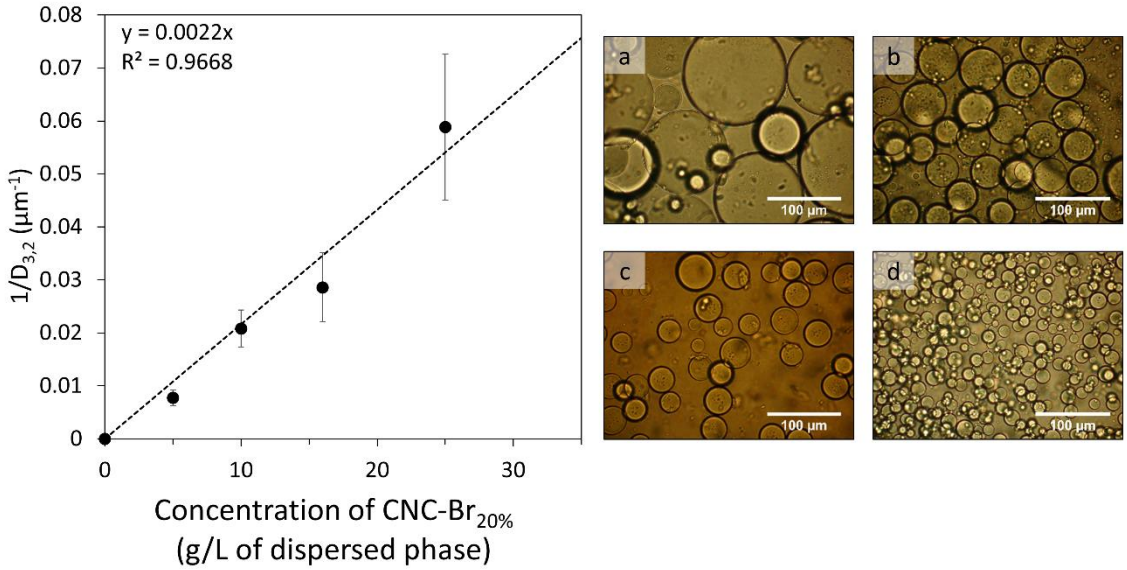

Figure 3 : Left, Reverse drop diameter as a function of the amount of CNC-$Br_{20\%}$ in the aqueous phase. All the other parameters are kept constant: 25/75$_{v/v}$ of IPM/polymerization system, OEGMA 40 wt% no TEGDA. The linear variation highlights the limited coalescence phenomenon occurring in this concentration range. Right, optical microscopy shots of the emulsions with a) 5 g/L, b) 10 g/L, c) 16 g/L, d) 25 g/L of CNC-$Br_{20\%}$.

The plot shows a linear dependence of the inverse of the diameter with the CNC-$Br_{20\%}$ particle concentration, which is characteristic of the behavior of Pickering emulsions. Indeed, in the

particle-poor domain, the size can be controlled by the amount of particles thanks to the limited coalescence phenomenon, because of the irreversible adsorption of particles at the oil-water interface (Arditty et al., 2003; Wiley, 1954). From the slope, it is possible to extract the covering ratio (C parameter), which is defined as the proportion of interface covered by particles. The slope is defined as (Schmitt et al., 2014) (Eq. 5):

$$\frac{1}{D_{3,2}} = \frac{m_p}{6\rho_p V_d C} \cdot \frac{a_p}{v_p} \qquad \textit{Eq. 5}$$

where a_p and v_p are the projected surface and the volume of the particles in contact with the interface (140x25 nm² and 140x25x25 nm³ respectively, approximating the CNC shape to a parallelepiped rectangle), m_p corresponds to the mass of particles, ρ_p their density (taken as 1.6 g/cm³), V_d the volume of the dispersed phase, and C the covering ratio. In the case of CNCs, which can be approximated to parallelepiped particles, a dense monolayer corresponds to a C value of 1. When C>1, the droplets are covered in average by n layers of particles, with C = n x 100 %. Here from the slope, it can be extracted that emulsions droplets are covered by 2 layers of CNCs in average. The formulation of the direct emulsion allows reaching stable emulsions droplets with mean diameters down to 17 µm, which makes them suitable as inner droplets for the double emulsion formulation. Indeed, previous attempts of formulating simple inverse emulsions of the same composition (water phase composed of 40 wt% of OEGMA) enabled producing droplets of average diameter of 400 µm (Dupont, Laurichesse, et al., 2021). It can therefore be assumed that the drops size of the second emulsification will be in the same range and thus suitable for the production of nicely defined double emulsions.

3.2.2 Double emulsion O/W/O

Double emulsions containing the monomers were formulated following a two-step emulsification process, with CNC-Br stabilizing each one of the two interfaces. According to previous characterizations, CNC-$Br_{20\%}$ were used to stabilize the O/W inner emulsion interface, and CNC-$Br_{90\%}$ for the outer interface. The simple direct emulsion was first formulated as described in the section 3.2.1 and used as dispersed phase for the second emulsification. By

changing the oil-to-water volume fraction of the direct emulsion, the loading fraction of inner droplets within the double emulsion could be tuned (Eq. 6).

$$n_{inner} = \varphi_{oil} \times \frac{{D_{4.3}}^3}{{d_{4.3}}^3} \quad \textit{Eq. 6}$$

with n_{inner} the average number of inner droplets, φ_{oil} the oil volume fraction of the direct emulsion, $D_{4,3}$ the volume averaged diameter of the external drops and $d_{4,3}$ the volume-averaged diameter of the inner droplets defined as $\mathrm{D}_{4,3} = \frac{\sum_i \mathrm{N_i D_i^4}}{\sum_i \mathrm{N_i D_i^3}}$.

Regarding the process, the choice of the second emulsification was determinant as it must not induce the modification, neither fragmentation nor destabilization of the inner emulsion. As a consequence, several mixing procedures were considered, with shear rates lower than the one induced by the ultrasonic probe used for the first emulsification (Ding et al., 2019). Rotor-stator, mechanical stirring and vibrating mixer were tested. In order to assess the stability of the double emulsion, the oil dispersed in the direct emulsion was stained with Nile Red (solubility in water 0.2 mg/mL), and the repartition of the dye after the second emulsification was used as a macroscopic indicator for process viability. More precisely, if the dye was finally present in the continuous phase, then it was assumed that the innermost and outer oily phases have been in contact during the emulsification process. This has to be avoided to prevent dilution of the active to be encapsulated and as a consequence to prevent low encapsulation efficiencies. At the microscopic scale, double emulsions were observed by optical microscopy and the average number of inner droplets was coarsely compared to the theoretical expected value n_{inner} (Eq. 6). Firstly, a rotor-stator Ultra-turrax® emulsification at low power (5000 rpm for 30 s) was employed (Figure 4 a, b). The direct emulsification led to empty double emulsions, similar to inverse emulsions. Therefore, a manual pre-mixing step was added to follow the emulsion evolution step-by-step. After a gentle manual premixing, the external oil was already stained with Nile Red (Figure 4 d), meaning that the emulsification did rupture some of the droplets of the direct emulsion. Regarding the morphology, the effective number of encapsulated inner droplets was already far from the theoretical value of a 250 droplets estimated by Eq. 6. After

further stirring using the Ultra-Turrax® rotor–stator mixer, the staining in the continuous oil phase intensified, and no inner droplet was visible anymore (Figure 4 e). Similarly, mechanical stirring ended up in the destabilization of the direct emulsion and an intense coloration was visible in the continuous phase after the second emulsification step (Figure 4 g).

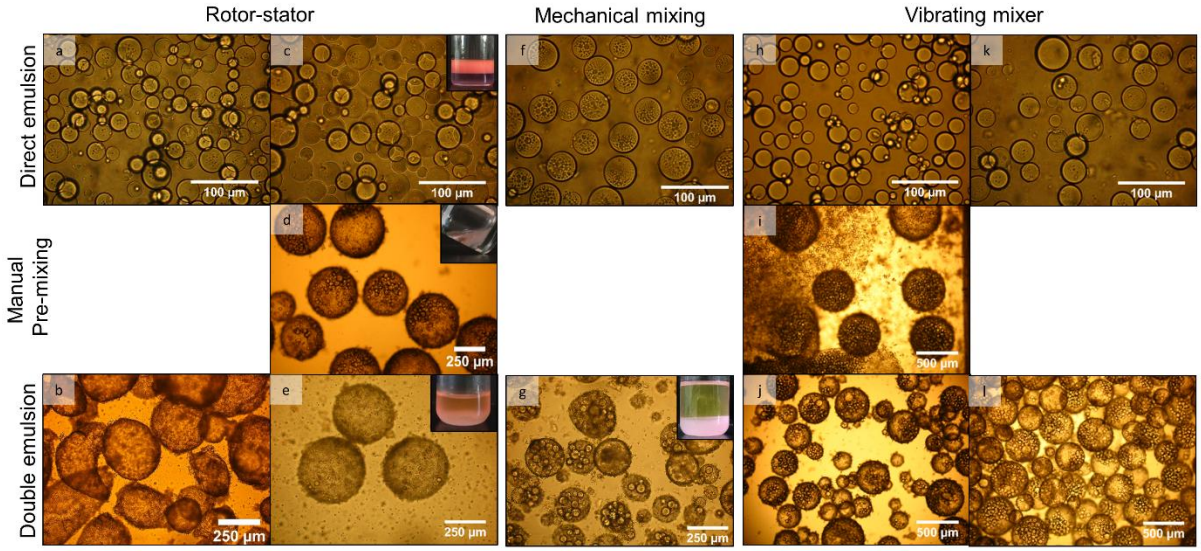

Figure 4 : Process optimization for emulsion formulation. a, b) direct and double emulsions from rotor-stator mixing. c, d, e) direct, premix and double emulsions from rotor-stator mixing. f,g) direct and double emulsions from mechanical stirring. h,i,j) direct, premix and double emulsions from vibrating mixer stirring. k,l) direct and double emulsions from vibrating mixer stirring. The inserts, when present, show the macroscopic aspect of the emulsion containing Nile Red.

Finally, a gentler process was chosen, and emulsification with a vibrating mixer (1500 rpm for 30 s) showed good results upon the double emulsion formulation, provided the suppression of the manual pre-mixing step (Figure 4 l). The inner emulsion average droplet diameter is preserved during the emulsification, as it is equal to 38 ± 7 µm before and 40 ± 7 µm after (Figure 5 left). Moreover, the CNC-$Br_{90\%}$ were efficiently adsorbed at the newly created water-oil interface as no sign of excess particles could be seen in the continuous phase.

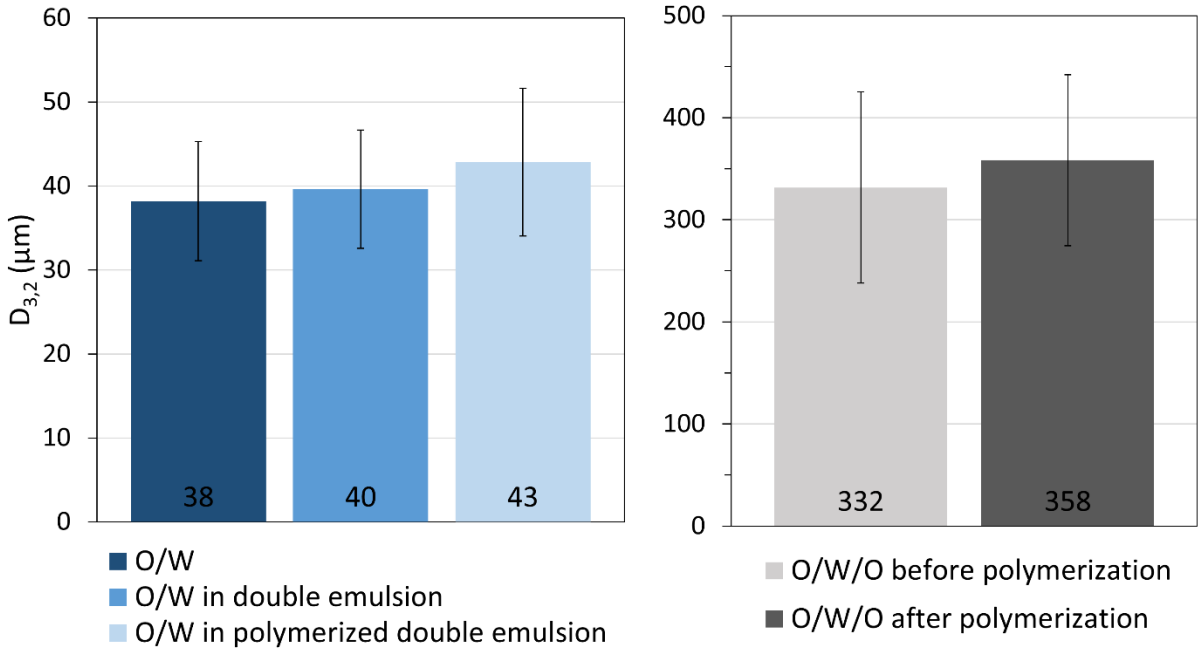

Figure 5: Left) inner droplets size distribution evolution after formulation, after incorporation in the double emulsion and after polymerization of the double emulsion. Right) double emulsion size distribution evolution before and after polymerization. The error bars reflect the drops size distribution width (standard deviation).

By setting the OEGMA concentration to 40 wt% in the aqueous phase, the concentration of CNC-$Br_{90\%}$ was varied and the according diameter of the double emulsion was measured. By plotting the inverse of the drop diameter as a function of the concentration of CNC-$Br_{90\%}$, a linear relationship characteristic of the limited coalescence phenomenon could be evidenced at the drop scale (Figure 6). In a previous contribution (Dupont, Laurichesse, et al., 2021), inverse simple emulsions of a 40 wt% OEGMA solution-in-IPM stabilized by CNC-$Br_{90\%}$ were obtained by homogenization with a rotor-stator, Ultra-turrax® S18N-10G at 15 000 rpm for 30 s. Interestingly, for identical CNC-$Br_{90\%}$ concentrations range, the average emulsion drop diameter was higher for these simple inverse emulsions than for the present double emulsion system (Fig. S2, SI), whereas the opposite was expected since the rotor-stator homogenization is more powerful than the vibrating mixer process. The ability of the CNC to adsorb at the interface is therefore influenced by the presence of the direct inner emulsion and is not only governed by the amount of particles and the power of homogenization. Indeed, in a previous contribution, it has been demonstrated that 41 layers of CNC-$Br_{90\%}$ were present on the inverse

emulsions surface (Dupont, Laurichesse, et al., 2021), and in the present case only half this value are adsorbed for each double emulsion drop. This difference could also be influenced by the change in the physical-chemical characteristics such as its viscosity of the dispersed phase, for instance.

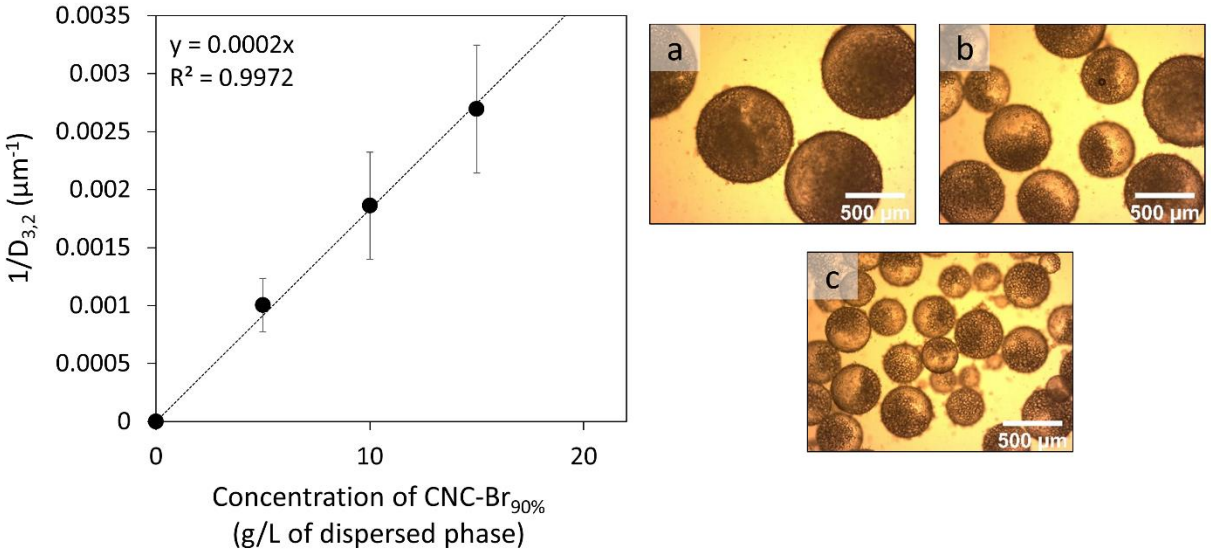

Figure 6 : Left, Reverse drop diameter as a function of the amount of CNC-Br$_{90\%}$ in the organic continuous phase. All the other parameters are kept constant: 25/75$_{v/v}$ of direct emulsion/IPM, direct emulsion IPM/aqueous phase ratio of 25/75$_{v/v}$, OEGMA 40 wt% no TEGDA. The linear variation highlights the limited coalescence phenomenon occurring in this concentration range. The error bars reflect the drops size distribution width (standard deviation). Right, optical microscopy shots of the double emulsions with a) 5 g/L, b) 10 g/L, c) 15 g/L of CNC-Br$_{90\%}$.

Similarly to simple emulsions, a covering ratio could be extracted here from the slope of the linear relationship between the inverse of the drop diameter and the concentration of particles (Figure 6), acknowledging an average of 21 layers of CNC-Br$_{90\%}$ at the drops surface. These multilayers are visible by optical microscopy, but more accurately by SEM (Figure 6, Figure 8), showing a rough solid interface and the presence of CNC aggregates. Regarding the morphology of the double emulsions, optical microscope observation showed that the inner droplets tend to stack at the outer droplet interface (Figure 7B f). This phenomenon can be explained by the van der Waals attractive interactions between the inner droplets and the wall formed by the outer drop surface (Sengupta & Papadopoulos, 1992; Wen et al., 2004). This observation is less visible when increasing the inner droplet volume fraction from 25 vol% to 50 vol%. Indeed, as the concentration of inner droplets increases, more volume of the drop is occupied and the segregation becomes less noticeable (Figure 7B g).

The aqueous intermediate phase composition could be varied, without disturbing the simple and double emulsion stability (Figure 7A). Stable double emulsions were obtained with different OEGMA concentration of 10 wt% or 40 wt% (Figure 7B a, e and b, f). The addition of TEGDA as a cross-linker to the aqueous solution of OEGMA (concentration of 5 wt% and 35 wt% respectively) did not impact neither the direct nor the double emulsion size (Figure 7B d, h, Figure 7A).

	Inner emulsion O/W volume faction (v/v)	OEGMA (wt%)	TEGDA (wt%)	Inner emulsion diameter (µm)	Double emulsion diameter (µm)
a,e	25/75	10	0	33 ± 8	350 ± 89
b,f	25/75	40	0	35 ± 8	377 ± 107
c,g	50/50	40	0	38 ± 9	332 ± 94
d,h	25/75	35	5	34 ± 9	377 ± 88

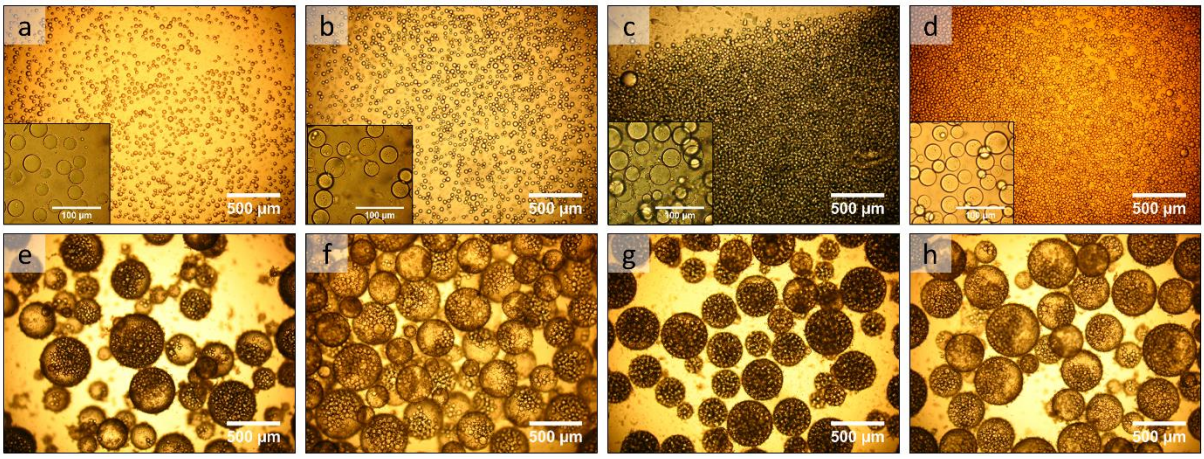

Figure 7: A) Formulation details of the emulsions presented below. B) Observation by optical microscopy of direct simple emulsion, 16 g/L CNC-Br$_{20\%}$, at low oil volume fraction 25/75$_{v/v}$ with varying OEGMA concentration a) 10 wt%, b) 40 wt%, c) with high oil volume fraction of 50/50$_{v/v}$, and d) in presence of a cross-linker (OEGMA/TEGDA 35/5 wt%). e-h) Respective double emulsions formulated with 20 g/L of CNC-Br$_{90\%}$.

3.3 Emulsion polymerization

Double emulsions were formulated with varying concentrations of OEGMA and TEGDA in the aqueous phase (10 wt%, 35 wt%-5wt%, 40wt%) and with two different loading fractions of inner droplets (25 vol% n_{inner}~250, 50 vol% n_{inner}~500). They were further polymerized by immersion in an oil bath at 75°C for 24 h. After polymerization, the emulsions were still dispersible in the supernatant IPM, contrary to observation of OEGMA/TEGDA polymerized emulsions initially stabilized by surfactants, which could only be redispersed in an aqueous medium (Stasse et al., 2020). Optical microscope observation showed a good stability of the

double emulsions upon heating and polymerization as the spherical morphology (Figure 8) and the mean diameters of both inner droplets and outer drops were preserved (Figure 5). Both internal droplets and external drops kept their average size distribution meaning that no coalescence nor destabilization events occurred during the polymerization process. For low loading fraction of inner droplets, the sticking phenomenon observed on non-polymerized double emulsions is even more visible after polymerization, with a clear segregation of the inner droplets on one side of the double emulsion, resulting in “Janus-like” polymer beads (Figure 8 a, b, d). The phenomenon induced by the van der Waals attractive interactions was most certainly enhanced by the creaming of the oil droplets within the drops during the 24h of polymerization, which were performed without mixing. Morphologies were further characterized by SEM, to assess the behavior of the capsules under a dry state and under vacuum (Figure 8 e-h). As it was previously observed for polymerized inverse emulsions (Dupont, Laurichesse, et al., 2021), the polymerized double emulsions presented on their surface a dense cover of CNCs, which might participate in the good redispersibility of the emulsions in IPM after polymerization. Almost all capsules could withstand the vacuum of the SEM chamber (10^{-5} Pa) without collapsing, except for the lowest OEGMA concentration (10 wt%), most certainly because of the low filling in polymer inside the aqueous core (Figure 8 e). For higher concentration in macromonomer, the objects kept their spherical shape with no deformation induced by the vacuum. The capsules were hand-cut to inspect their inner core. As expected, matrix morphology was observed, with visible cavities assessing for the presence of the oil inner droplets (Figure 8 f, g, h). For low loading fractions of inner droplets about 25 vol% (Figure 8 f, g), the repartition of the cavities is clearly segmented with one part of the capsule composed of full polymer and the other side concentrating the cavities made from the presence of inner oil droplets. The increase in the inner droplet loading fraction from 25 vol% to 50 vol% (Figure 8 g) is visible with an increase in the average number of cavities per capsule, but also from the more even repartition of the cavities within the capsule, less subjected to the microscopic segregation due to the van der Waals interactions.

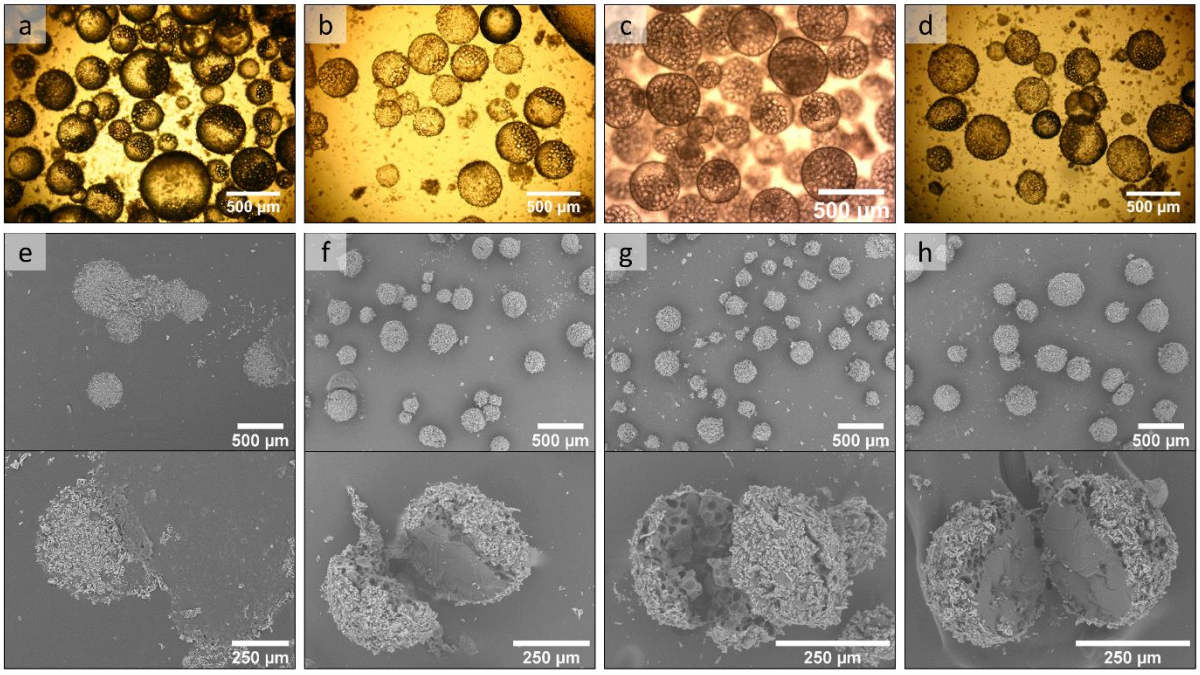

Figure 8: Optical microscopy images of polymerized emulsions with 25 %v inner oil and a) 10 wt% OEGMA, b) 40 wt% OEGMA, d) 35 wt% OEGMA and 5 wt% TEGDA, and c) with 50 %v inner oil and 40 wt% OEGMA. e-h) SEM pictures of the respective polymerized double emulsions, from a low and high magnification.

3.4 Encapsulation efficiency

Double emulsions of OEGMA and TEGDA were efficiently stabilized by CNCs and further polymerized to obtain well-defined solid capsules. To increase the impact of these objects, their encapsulation ability was assessed as a proof of concept. The choice of encapsulated species was orientated towards fluorescent dyes (as models) which can be easily followed visually by confocal microscopy and quantified by UV-Vis spectrophotometry. The hydrophobic dye FY131SC, which is composed of “Solvent Red 175” dye, was chosen because of its very low solubility in water, with a maximum of absorption at 530 nm (full absorbance spectrum Fig. S3, SI). Its addition to IPM did not impact the emulsion formulation (Figure 9 a, b), since both droplets and drops average diameter were equal to 47 ± 8 µm and 367 ± 103 µm respectively without dye and to 38 ± 9 µm, 332 ± 94 µm respectively in presence of FY131SC. The choice of the hydrophilic dye was subjected to optimization as it should have a different range of maximum of absorption and emission than the hydrophobic one, but also should not present interfacial properties in order not to interfere with the emulsion formulation. Therefore, toluidine

blue was preferred since it did not induce any change in the double emulsion formulation (Figure 9 c, d), contrary to other dyes like methylene blue which contributed in increasing the direct emulsion droplet diameter (Fig. S4, SI).

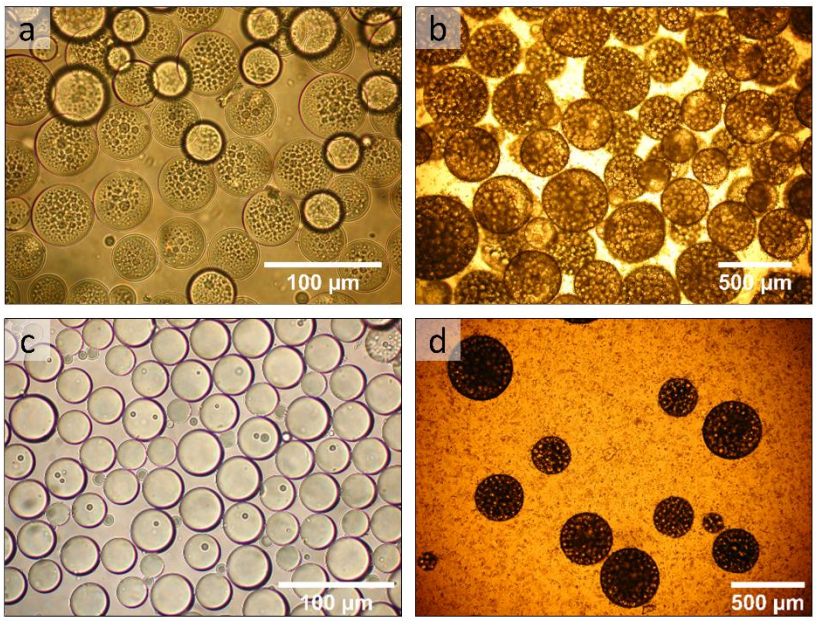

Figure 9: Optical microscopy picture of direct (a,c) and corresponding double emulsion (b,d) in presence of a, b) FY131SC and c, d) both FY131SC and toluidine blue.

Confocal microscopy observation was performed on the stabilized double emulsion to verify the effectiveness of the encapsulation and the special repartition of both dyes. Emulsions were imaged by transmitted light and by fluorescence on a medium plane to enable the visualization of the inner droplets. Each dye was imaged on a separate channel (hydrophobic FY131SC appears in green and hydrophilic toluidine blue appears in red) and both signals were merged by computation. The experiment shows that both toluidine blue and FY131SC are present in the aqueous and oil phase of the direct emulsion respectively (Figure 10 i). For the double emulsion, the inner droplets can be easily distinguished from the intermediate polymerized phase as they are selectively labelled by the hydrophobic dye (Figure 10 g). The polymer phase, which appears red is also selectively stained by the hydrophilic dye (Figure 10 f). Another feature which might be of interest to notice is the light green staining in the background assessing for the presence of the hydrophobic dye in the continuous phase, and indicating the occurrence of leakage following the second emulsification. However, as the fluorescence intensity in the background is low compared to the inner droplets, the concentration of dye in

the continuous phase can be considered as low and therefore that the leakage is not too pronounced.

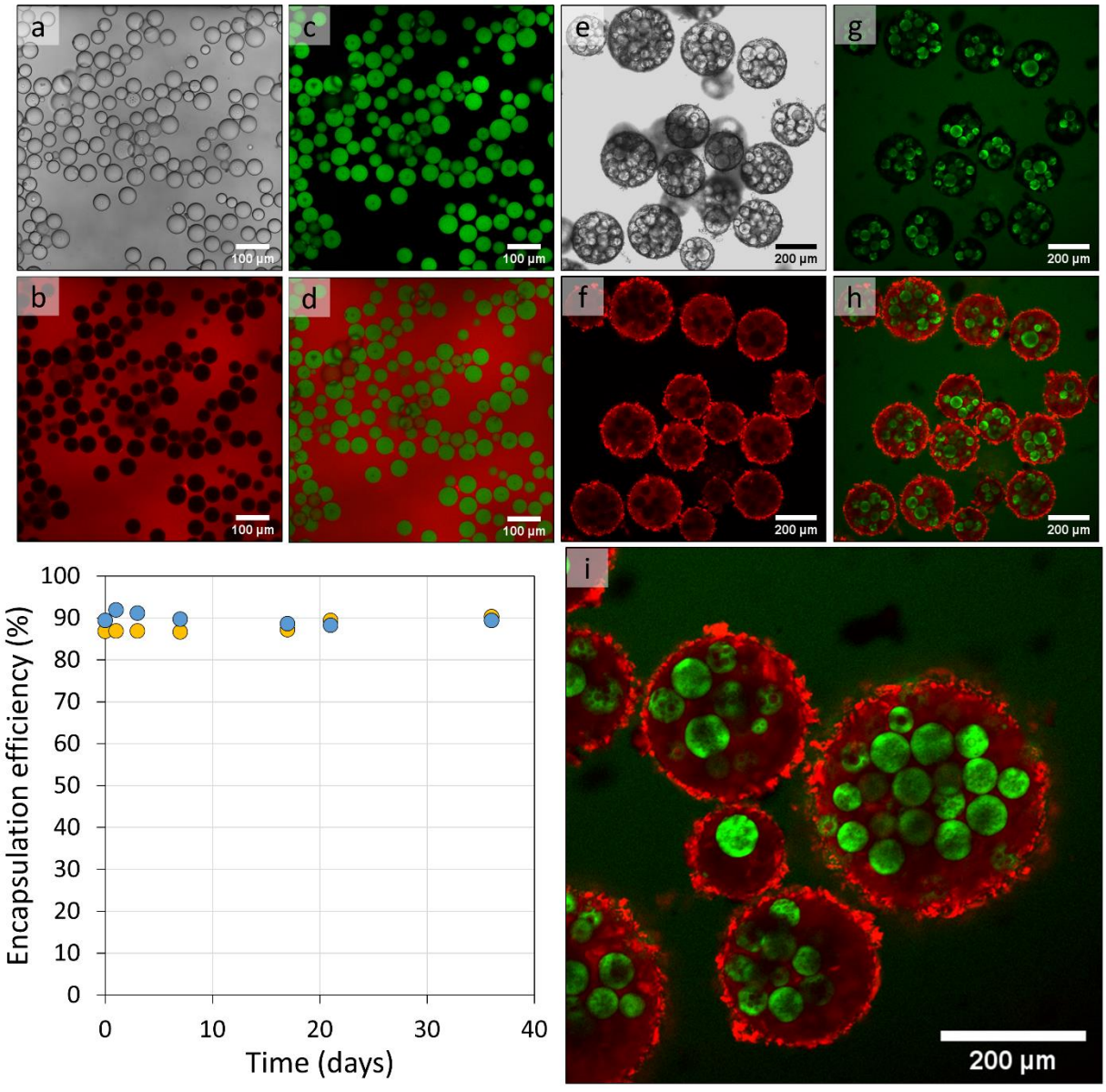

Figure 10: Pictures – Confocal microscopy image of a direct emulsion with toluidine blue and FY131SC, a) in bright field, b) red channel, c) green channel and d) superimposition of the red and green channels. Toluidine blue and FY131SC are revealed by the red and green channels respectively. e-h) Resulting double emulsion with toluidine blue and FY131SC, and i) close-up at higher magnification. Images were taken at a given z. Graph – Encapsulation efficiency of double emulsions of OEGMA and TEGDA, with (blue) and without (yellow) polymerization. The point at t = 0 corresponds to the sample right after formulation, and t = 1 day corresponds to the sample after 24h of polymerization for the blue curve.

In order to corroborate this hypothesis, and quantify the amount of dye that could effectively be encapsulated within the double emulsion-templated capsules, indirect encapsulation efficiency measurement was performed. Double emulsions with FY131SC in the inner oil droplets were formulated with 35 wt% OEGMA and 5 wt% TEGDA in the intermediate phase.

One double emulsion was kept at ambient temperature as a control experiment, while the other was polymerized at 75°C for 24h. The presence of dye in the IPM continuous phase was measured over time by UV-Visible spectrophotometry. Thanks to Eq. 4, the encapsulation efficiency was calculated for both non-polymerized and polymerized double emulsions. Both double emulsions showed good encapsulation efficiency of about 90% directly after formulation (Figure 10). After polymerization, almost no dye could be detected into the continuous phase, giving an estimated encapsulation efficiency of about 90% (Figure 10, blue). A control experiment has been additionally performed, and has shown that the hydrophobic dye does not degrade when submitted to 75°C during 24h (Figure S5, SI). Hence, the absence of dye detection into the continuous phase can be accurately linked to the good encapsulation efficiency and not to a dye leakage followed by degradation. This encapsulation efficiency value remained constant over a month, for both the non-polymerized and the polymerized double emulsions. Hence, the polymerization process of the double emulsion, even in harsh conditions of temperature, did not affect neither the stability of the system nor the encapsulation efficiency of the hydrophobic dye, which is promising regarding active-delivery applications.

4. Conclusion

We have shown that O/W/O double emulsions could be stabilized using solely brominated cellulose nanocrystals. Their modification rate was directly linked to the reaction time, and monitors the ability of the particles to stabilize either direct or inverse emulsion. Double emulsion could be formulated using two batches of CNCs, one with a low modification rate about 20% and the other with a high modification rate of 90%. Isopropyl myristate, a polar biocompatible oil was used as inner oil phase and as continuous medium. The aqueous intermediate phase was composed of oligoethylene glycol derivatives, namely hydroxyl oligoethylene glycol methacrylate and tertraethylene glycol diacrylate. For the first time, a double emulsion stabilized solely by CNCs was polymerized. The aqueous intermediate phase was polymerized by free radical polymerization, and led to solid matrix capsules, which

conserved the initial emulsion characteristics, with tunable inner droplets content, and varying monomer(s) fraction. Finally, their use as double encapsulation vessels was investigated. Both hydrophobic and hydrophilic dyes could be encapsulated within the inner droplets and the intermediate phase respectively. The encapsulation efficiency of the hydrophilic dye was equal to 100% given the insolubility of the dye in the other phases. For the hydrophobic dye, it was measured approximately equal to 90% indicating promising results to further extend their application to controlled delivery.

Acknowledgements

The authors would like to thank Emmanuel Ibarboure for his help with fluorescence microscopy imaging of the stained emulsions.

This work was supported by the French “Fondation Bordeaux Université” and the “Fonds Ernest Solvay” supported by “Fondation Roi Baudouin”.

References

Arditty, S, Whitby, C. P., Binks, B. P., Schmitt, V., & Leal-Calderon, F. (2003). Some general features of limited coalescence in solid-stabilized emulsions. *Eur. Phys. J. E*, *11*, 273–281. https://doi.org/10.1140/epje/i2003-10018-6

Arditty, Stéphane, Schmitt, V., Giermanska-Kahn, J., & Leal-Calderon, F. (2004). Materials based on solid-stabilized emulsions. *Journal of Colloid and Interface Science*, *275*, 659–664. https://doi.org/10.1016/j.jcis.2004.03.001

Brand, J., Pecastaings, G., & Sèbe, G. (2017). A versatile method for the surface tailoring of cellulose nanocrystal building blocks by acylation with functional vinyl esters. *Carbohydrate Polymers*, *169*, 189–197. https://doi.org/10.1016/j.carbpol.2017.03.077

Cunha, A. G., Mougel, J.-B., Cathala, B., Berglund, L. A., & Capron, I. (2014). Preparation of double Pickering emulsions stabilized by chemically tailored nanocelluloses. In *Langmuir* (Vol. 30). https://doi.org/10.1021/la5017577

Deng, Z., Jung, J., Simonsen, J., & Zhao, Y. (2018). Cellulose nanocrystals Pickering emulsion incorporated chitosan coatings for improving storability of postharvest Bartlett pears (Pyrus communis) during long-term cold storage. *Food Hydrocolloids*, *84*, 229–237. https://doi.org/10.1016/J.FOODHYD.2018.06.012

Destribats, M., Gineste, S., Laurichesse, E., Tanner, H., Leal-Calderon, F., Héroguez, V., & Schmitt, V. (2014). Pickering Emulsions: What Are the Main Parameters Determining the Emulsion Type and Interfacial Properties? *Langmuir*, *30*, 9313–9326. https://doi.org/10.1021/la501299u

Ding, S., Serra, C. A., Vandamme, T. F., Yu, W., & Anton, N. (2019). Double emulsions prepared by two–step emulsification: History, state-of-the-art and perspective. In *Journal of Controlled Release* (Vol. 295, pp. 31–49). Elsevier B.V. https://doi.org/10.1016/j.jconrel.2018.12.037

Dupont, H., Fouché, C., Dourges, M.-A., Schmitt, V., & Héroguez, V. (2020). Polymerization of cellulose nanocrystals-based Pickering HIPE towards green porous materials. *Carbohydrate Polymers*, *243*, 116411. https://doi.org/10.1016/j.carbpol.2020.116411

Dupont, H., Laurichesse, E., Héroguez, V., & Schmitt, V. (2021). Green Hydrophilic Capsules from Cellulose Nanocrystal-Stabilized Pickering Emulsion Polymerization: Morphology Control and Spongelike Behavior. *Biomacromolecules*, *22*(8), 3497–3509. https://doi.org/10.1021/acs.biomac.1c00581

Dupont, H., Maingret, V., Schmitt, V., & Héroguez, V. (2021). New Insights into the Formulation and Polymerization of Pickering Emulsions Stabilized by Natural Organic Particles. *Macromolecules*, *54*(11), 4945–4970. https://doi.org/10.1021/acs.macromol.1c00225

Finkle, P., Draper, H. D., & Hildebrand, J. H. (1923). The Theory of Emulsification. *Journal of American Chemical Society*, *45*(12), 2780–2788. https://pubs.acs.org/sharingguidelines

Gestranius, M., Stenius, P., Kontturi, E., Sjöblom, J., & Tammelin, T. (2017). Phase behaviour and droplet size of oil-in-water Pickering emulsions stabilised with plant-derived nanocellulosic materials. *Colloids and Surfaces A: Physicochemical and Engineering Aspects*, *519*, 60–70. https://doi.org/10.1016/j.colsurfa.2016.04.025

Gonzalez Ortiz, D., Pochat-Bohatier, C., Cambedouzou, J., Bechelany, M., & Miele, P. (2020). Current Trends in Pickering Emulsions: Particle Morphology and Applications. *Engineering*. https://doi.org/10.1016/j.eng.2019.08.017

Guo, J., Du, W., Gao, Y., Cao, Y., & Yin, Y. (2017). Cellulose nanocrystals as water-in-oil Pickering emulsifiers via intercalative modification. *Colloids and Surfaces A: Physicochemical and Engineering Aspects*, *529*, 634–642. https://doi.org/10.1016/j.colsurfa.2017.06.056

Hedjazi, S., & Razavi, S. H. (2018). A comparison of Canthaxanthine Pickering emulsions, stabilized with cellulose nanocrystals of different origins. *International Journal of Biological Macromolecules*, *106*, 489–497. https://doi.org/10.1016/j.ijbiomac.2017.08.030

Kalashnikova, I., Bizot, H., Cathala, B., & Capron, I. (2011). New Pickering Emulsions Stabilized by Bacterial Cellulose Nanocrystals. *Langmuir*, *27*(12), 7471–7479. https://doi.org/10.1021/la200971f

Lee, K.-Y., Blaker, J. J., Murakami, R., Heng, J. Y. Y., & Bismarck, A. (2013). *Phase Behavior of Medium and High Internal Phase Water-in-Oil Emulsions Stabilized Solely by Hydrophobized Bacterial Cellulose Nanofibrils*. https://doi.org/10.1021/la4032514

Mackie, A., Gourcy, S., Rigby, N., Moffat, J., Capron, I., & Bajka, B. (2019). The fate of cellulose nanocrystal stabilised emulsions after simulated gastrointestinal digestion and exposure to intestinal mucosa †. *Nanoscale*, *11*. https://doi.org/10.1039/c8nr05860a

Matos, M., Timgren, A., Sjöö, M., Dejmek, P., & Rayner, M. (2013). Preparation and encapsulation properties of double Pickering emulsions stabilized by quinoa starch granules. *Colloids and Surfaces A: Physicochemical and Engineering Aspects*, *423*, 147–153. https://doi.org/10.1016/j.colsurfa.2013.01.060

Meng, T., Gao, X., Zhang, J., Yuan, J., Zhang, Y., & He, J. (2008). Graft copolymers prepared by atom transfer radical polymerization (ATRP) from cellulose. *Polymer*, *50*, 447–454. https://doi.org/10.1016/j.polymer.2008.11.011

Morandi, G., Heath, L., & Thielemans, W. (2009). Cellulose Nanocrystals Grafted with Polystyrene Chains through Surface Initiated Atom Transfer Radical Polymerization (SI-ATRP). *Langmuir*, *25*(14), 5. https://doi.org/10.1021/la900452a

Pan, J., Yin, Y., Gan, M., Meng, M., Dai, X., Wu, R., Shi, W., & Yan, Y. (2015). Fabrication and evaluation of molecularly imprinted multi-hollow microspheres adsorbents with tunable inner pore structures derived from templating Pickering double emulsions. *Chemical Engineering Journal*, *266*, 299–308. https://doi.org/10.1016/J.CEJ.2014.11.126

Pickering, S. U. (1907). CXCVI.—Emulsions. *Journal of the Chemical Society, Transactions, 91*, 2001–2021.

Ramsden, W. (1904). Separation of solids in the surface-layers of solutions and 'suspensions' (observations on surface-membranes, bubbles, emulsions, and mechanical coagulation).—Preliminary account. *Proceedings of the Royal Society of London*, *72 (477-48*, 156–164.

Sarkar, A., & Dickinson, E. (2020). Sustainable food-grade Pickering emulsions stabilized by

plant-based particles. *Current Opinion in Colloid & Interface Science*, *49*, 69–81. https://doi.org/10.1016/j.cocis.2020.04.004

Schmitt, V., Destribats, M., & Backov, R. (2014). Colloidal particles as liquid dispersion stabilizer: Pickering emulsions and materials thereof. *Comptes Rendus Physique*, *15*(8–9), 761–774. https://doi.org/10.1016/j.crhy.2014.09.010

Sengupta, A. K., & Papadopoulos, K. D. (1992). van der Waals Interaction between a Colloid and the Wall of Its Host Spherical Cavity. *Journal of Colloid and Interface Science*, *152*(2), 534–542.

Spyropoulos, F., Duffus, L. J., Smith, P., & Norton, I. T. (2019). Impact of Pickering Intervention on the Stability of W1/O/W2 Double Emulsions of Relevance to Foods. *Langmuir*, *35*, 15137–15150. https://doi.org/10.1021/acs.langmuir.9b01995

Stasse, M., Laurichesse, E., Vandroux, M., Ribaut, T., Héroguez, V., & Schmitt, V. (2020). Cross-linking of double oil-in-water-in-oil emulsions: A new way for fragrance encapsulation with tunable sustained release. *Colloids and Surfaces A: Physicochemical and Engineering Aspects*, *607*, 125448. https://doi.org/10.1016/j.colsurfa.2020.125448

Wen, L., Cheng, J., Zou, H., Zhang, L., Chen, J., & Papadopoulos, K. D. (2004). van der Waals Interaction between Internal Aqueous Droplets and the External Aqueous Phase in Double Emulsions. *Langmuir*, *20*, 8391–8397. https://doi.org/10.1021/la049353s

Werner, A., Schmitt, V., Sèbe, G., & Héroguez, V. (2019). Convenient Synthesis of Hybrid Polymer Materials by AGET-ATRP Polymerization of Pickering Emulsions Stabilized by Cellulose Nanocrystals Grafted with Reactive Moieties. *Biomacromolecules*, *20*(1), 490. https://doi.org/10.1021/acs.biomac.8b01482

Wiley, R. M. (1954). Limited coalescence of oil droplets in coarse oil-in-water emulsions. *Journal of Colloid Science*, *9*(5), 427–437. https://doi.org/10.1016/0095-8522(54)90030-6

Zhang, Z., Tam, K. C., Wang, X., & Sèbe, G. (2018). Inverse Pickering Emulsions Stabilized by Cinnamate Modified Cellulose Nanocrystals as Templates to Prepare Silica

624 Colloidosomes. *ACS Sustainable Chemistry and Engineering*, *6*(2), 2583–2590.
625 https://doi.org/10.1021/acssuschemeng.7b04061
626